THE ASTROPHYSICAL JOURNAL, 463:120–133, 1996 May 20

HUBBLE SPACE TELESCOPE OBSERVATIONS OF THE UNUSUAL BLUE COMPACT DWARF GALAXY MARKARIAN 996[1]

TRINH X. THUAN
Astronomy Department, University of Virginia, Charlottesville, VA 22903-0818; txt@virginia.edu

YURI I. IZOTOV
Main Astronomical Observatory, Ukrainian Academy of Sciences, Goloseevo, Kiev 252650, Ukraine; izotov@mao.gluk.apc.org

AND

VALENTIN A. LIPOVETSKY
Special Astrophysical Observatory, Russian Academy of Sciences, Nizhny Arkhyz, Karachai-Circessia 357147, Russia; val@sao.stavropol.su

Received 1995 June 22; accepted 1995 December 4

ABSTRACT

We present *Hubble Space Telescope* Wide Field Planetary Camera 2 *V* and *I* images and Faint Object Spectrograph UV and optical spectrophotometry of the unusual blue compact dwarf galaxy Mrk 996. We found Mrk 996 to have a disk structure with a small scale length (∼0.4 kpc) and a two-arm spiral-like pattern confined to the inner 160 pc in radius. Nearly all the star-forming activity occurs in an extremely compact nuclear H II region of radius ∼315 pc. A central density greater than 10^6 cm^{-3}, together with a density gradient, are needed to explain the emission-like intensities. The density gradient may be caused by a mass outflow, which would also account for the much broader line widths (FWHM ∼ 900 km s^{-1}) of the high-excitation lines originating in the inner region as compared with the low-excitation lines originating in the outer region. There is a large population of WR stars that may drive the mass outflow and heavily pollute the central region with nitrogen, producing a nitrogen abundance gradient from the inner to the outer parts. The nitrogen abundance in the center is about 25 times larger than that derived for other blue compact galaxies. It decreases by a factor of about 6 from the inner high-excitation zone to the outer low-excitation zone.

The number ratio of WNL stars to O stars is ≥0.1, larger by a factor of ≥5 than predictions by evolutionary synthesis models. The ratio of the number of WC stars to the total number of WR stars is ∼0.11. The oxygen abundance of Mrk 996 is ∼1/10 that of the Sun, its C/O ratio is 0.25, and its helium mass fraction $Y = 0.26$. There is a system of old (∼10^{10} yr) globular clusters distributed asymmetrically around Mrk 996, mainly to the south of the galaxy; an asymmetry probably related to the one seen in the outer isophotes of Mrk 996. The globular cluster luminosity function in Mrk 996 is very similar to that of the Milky Way, with a suggestion of a slightly larger number of clusters at the bright end, in the M_V range between −9 and −10.4.

Subject headings: galaxies: abundances — galaxies: compact — galaxies individual (Markarian 996) — galaxies: ISM — galaxies: nuclei — galaxies: stellar content — galaxies: structure

1. INTRODUCTION

In the course of an extensive study of blue compact dwarf galaxies (BCDs) to derive the primordial helium abundance (Izotov, Thuan, & Lipovetsky 1994, 1995), heavy-element abundances (Thuan, Izotov, & Lipovetsky 1995), and the BCD large-scale spatial distribution (Pustil'nik et al. 1995), our attention was drawn to the unusual properties of the dwarf emission-line galaxy Mrk 996, where star formation appears to occur exclusively in an extremely compact nuclear region. Discovered by Markarian, Lipovetsky, & Stepanian (1977), spectroscopic work by Denisyuk & Lipovetsky (1984) shows Mrk 996 to be a nearby dwarf galaxy with strong Hα emission.

A subsequent spectrum obtained by Izotov et al. (1992) with the Russian 6 m telescope showed the galaxy to have very unusual spectroscopic properties when compared with those of normal extragalactic H II regions: (1) The nuclear H II region shows a very high excitation. The temperature derived from the [O III] λ4363/(λ4959 + λ5007) emission-line intensity ratio in the case of a low-density photoionized H II region is unusually high, exceeding T_e = 20,000 K. The oxygen abundance derived in these physical conditions is extremely low, amounting to only 1/40 of the solar value. (2) The He I line intensities of the He I λ4471, λ5876, and λ6678 emission lines are 1.5–2 times larger, and that of the He I λ7065 line 4 times larger, than typical values in giant extragalactic H II regions. (3) Different ions show different line widths. Emission lines of low-ionization ions (O^+, S^+, N^+) have narrow line widths, while emission lines of higher ionization stages (all helium lines, the O^{++} and Ne^{++} nebular lines, and all auroral lines) show broader line widths (∼900 km s^{-1}). The correlation of line widths with ionization stages suggests different kinematical properties in different ionization zones that can be caused by a mass outflow.

The main observational properties of Mrk 996 are summarized in Table 1. At the adopted distance[2] of 21.6 Mpc, 1″ corresponds to a linear size of 105 pc. To better understand the nature of this extraordinary object, we have

[1] Based on observations obtained with the NASA/ESA *Hubble Space Telescope* through the Space Telescope Science Institute, which is operated by Association of Universities for Research in Astronomy (AURA), Inc., under NASA contract NAS 5-26555.

[2] We shall adopt throughout a Hubble constant of 75 km s^{-1} Mpc^{-1}.

TABLE 1

Observational Characteristics of Mrk 996

Parameter	Value
α(1950)	$01^h25^m04^s.5$
δ(1950)	$-06°35'08''$
l^{II}, b^{II}	147°, −67°
d_{25}[a]	34″.8
D (Mpc)	21.6
d (kpc)	3.67
B[b]	14.96
$U-B$[c]	−0.32
$B-V$[c]	0.44
$V-R$[c]	0.60
$V-I$[d]	0.75
M_B	−16.71
μ_V (mag arcsec^{-2})[e]	19.90
μ_I (mag arcsec^{-2})[e]	19.05
α^{-1} (kpc)[e]	0.42
$v_{\rm H\,I}$ (km s^{-1})[f]	1622 ± 10
Δv_{20} (km s^{-1})[f]	177 ± 25
Δv_{50} (km s^{-1})[f]	83 ± 25
$F_{\rm H\,I}$ (10^6 $M_\odot$)[f]	0.24
$M_{\rm H\,I}$ (10^8 $M_\odot$)[f]	1.12
L_B (10^8 $L_\odot$)	9.7
$M_{\rm H\,I}/L_B$ ($M_\odot/L_\odot$)	0.12

[a] Blue isophotal diameter at $B = 25$ mag arcsec^{-2} (this paper).
[b] Blue total magnitude corrected for Galactic extinction (this paper).
[c] Colors obtained through a 9″ diameter aperture, corrected for Galactic extinction (Izotov et al. 1993).
[d] Total color corrected for Galactic extinction (this paper).
[e] Disk parameters (this paper). The central surface brightnesses have been corrected for Galactic extinction.
[f] H I parameters (Thuan et al. 1995).

obtained imaging and spectroscopic observations of Mrk 996 with the refurbished *Hubble Space Telescope* (*HST*), in the course of a larger study of extremely metal-deficient BCDs with *HST*. The superior angular resolution of *HST* is ideal for studying the very compact star-forming nuclear region in the galaxy.

2. OBSERVATIONS AND DATA REDUCTION

2.1. *Imaging*

We obtained images of Mrk 996 on 1994 December 29 during cycle 4, after the refurbishment mission, with the *HST* Wide Field Planetary Camera 2 (WFPC2) in filters F569W and F791W, which we will refer to as V and I throughout the paper. Two exposures of equal duration were obtained in each filter to permit identification and removal of cosmic rays. The total exposure time was 1800 s in V and 4400 s in I. The scale of the WFPC2 is 0″.102 per pixel.

Preliminary processing of the raw images, including corrections for flat-fielding, was done at the Space Telescope Science Institute through the standard pipeline. Subsequent reductions were carried out at the University of Virginia using IRAF[3] and STSDAS.[4] Point sources in the processed images have a FWHM of ~2 pixels or 0″.2. Cosmic rays were removed, and the images in each filter were combined. We found that all exposures in a given filter coregistered to better than ~0.2 pixels. The very bright nucleus resulted in the saturation of the central 8 pixels in the V image and in the central 12 pixels in the I image. The transformation of instrumental magnitudes to the Johnson-Cousins *UBVRI* photometric system as defined by Landolt (1992) was performed according to the prescriptions of Holtzman et al. (1995):

$$V = \begin{cases} -2.5 \log ({\rm DN\ s^{-1}}) + 0.089(V-I) \\ \quad -0.002(V-I)^2 + 22.168, \quad (V-I) < 2.0\,, \\ -2.5 \log ({\rm DN\ s^{-1}}) - 0.124(V-I) \\ \quad +0.022(V-I)^2 + 22.499, \quad (V-I) \geq 2.0\,, \end{cases} \tag{1}$$

$$I = \begin{cases} -2.5 \log ({\rm DN\ s^{-1}}) - 0.028(V-I) \\ \quad -0.004(V-I)^2 + 21.458, \quad (V-I) < 1.0\,, \\ -2.5 \log ({\rm DN\ s^{-1}}) - 0.085(V-I) \\ \quad +0.011(V-I)^2 + 21.503, \quad (V-I) \geq 1.0\,, \end{cases} \tag{2}$$

where DN s^{-1} is the observed count rate.

Colors and magnitudes were derived by iterating on equations (1)–(2). The resulting measured brightness of the sky background is 22.2 mag arcsec^{-2} in V and 21.5 mag arcsec^{-2} in I.

2.2. *Spectrophotometry*

We also obtained UV and optical spectra of Mrk 996 with the Faint Object Spectrograph (FOS) during cycle 4 on 1995 January 26. The UV spectrum was obtained with grating G190H and an integration time of 1860 s, and covers the wavelength range 1572–2312 Å. The optical spectra were obtained with grating G400H and an exposure time of 960 s in the blue range (3235–4781 Å), and with grating G570H and an exposure time of 1320 s in the red range (4569–6818 Å). The spectra were taken consecutively in time with the 0″.86 circular aperture (aperture B-3) giving a spectral resolution of ~3 Å for the UV spectrum, ~6 Å for the blue spectrum, and ~9 Å for the red one.

The spectra were processed through the standard *HST* pipeline reductions, with corrections for flat-fielding, wavelength determination, instrumental background subtraction, and photometric calibration. The instrumental and sky backgrounds were negligible for our observations.

3. RESULTS

3.1. *Morphology*

We display, in Figure 1*a* (Plate 10), the V image with the contrast level adjusted so as to show the high surface brightness nuclear star-forming region and, in Figure 1*b* (Plate 11), the I image with the contrast level adjusted so as to show the low surface brightness underlying extended component. Figures 2*a* and 2*b* show the corresponding isophotal maps, in pixel coordinates. The bulk of the star formation occurs within a very compact, roughly circular region of ~3″ (~315 pc) radius. To the north, starting at $r \sim 2''$, there are dust patches extending over ~3″. The presence of the dust patches causes a deformation of the inner isophotal contours just outside of the star-forming region, which is clearly apparent in Figure 2. Surrounding the nuclear star-forming region are several pointlike sources that we shall discuss in § 3.3. Figure 1*b* shows that the

[3] The Image Reduction and Analysis Facility is distributed by the National Optical Astronomical Observatories, which are operated by the AURA, Inc., under cooperative agreement with the National Science Foundation (NSF).

[4] The Space Telescope Science Data Analysis System.

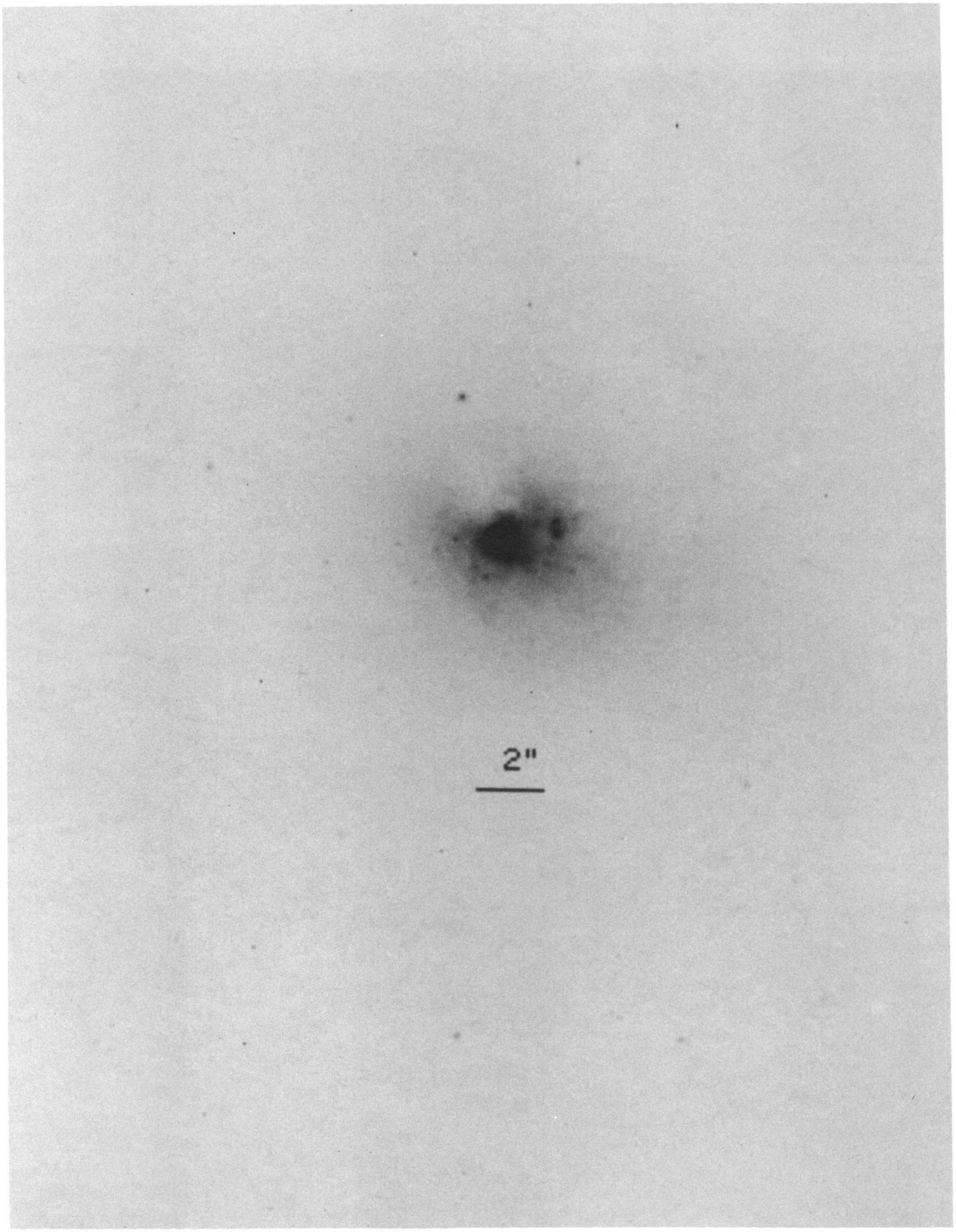

FIG. 1*a*

FIG. 1.—(*a*) A 1800 s *V* WFPC2 image of the BCD Mrk 996 taken with the refurbished *HST*, with the contrast adjusted to show the high surface brightness nuclear region. At a distance of 21.6 Mpc, 1″ corresponds to a linear scale of 105 pc. Dust patches can be seen ~3″ to the north of the nucleus. At 2″ to the west of the nuclear starburst, there is a separate star-forming region. Pointlike sources around the nucleus are globular clusters. The orientation is the same as in (*b*). (*b*) A 4400 s *I* WFPC2 image of Mrk 996 with the contrast adjusted to show the low surface brightness outer envelope of the galaxy. There is a distinct asymmetry in the spatial distribution of the globular cluster pointlike sources, which are mainly to the south of the galaxy. The envelope is also more extended toward the northern side.

THUAN, IZOTOV, & LIPOVETSKY (see 463, 121)

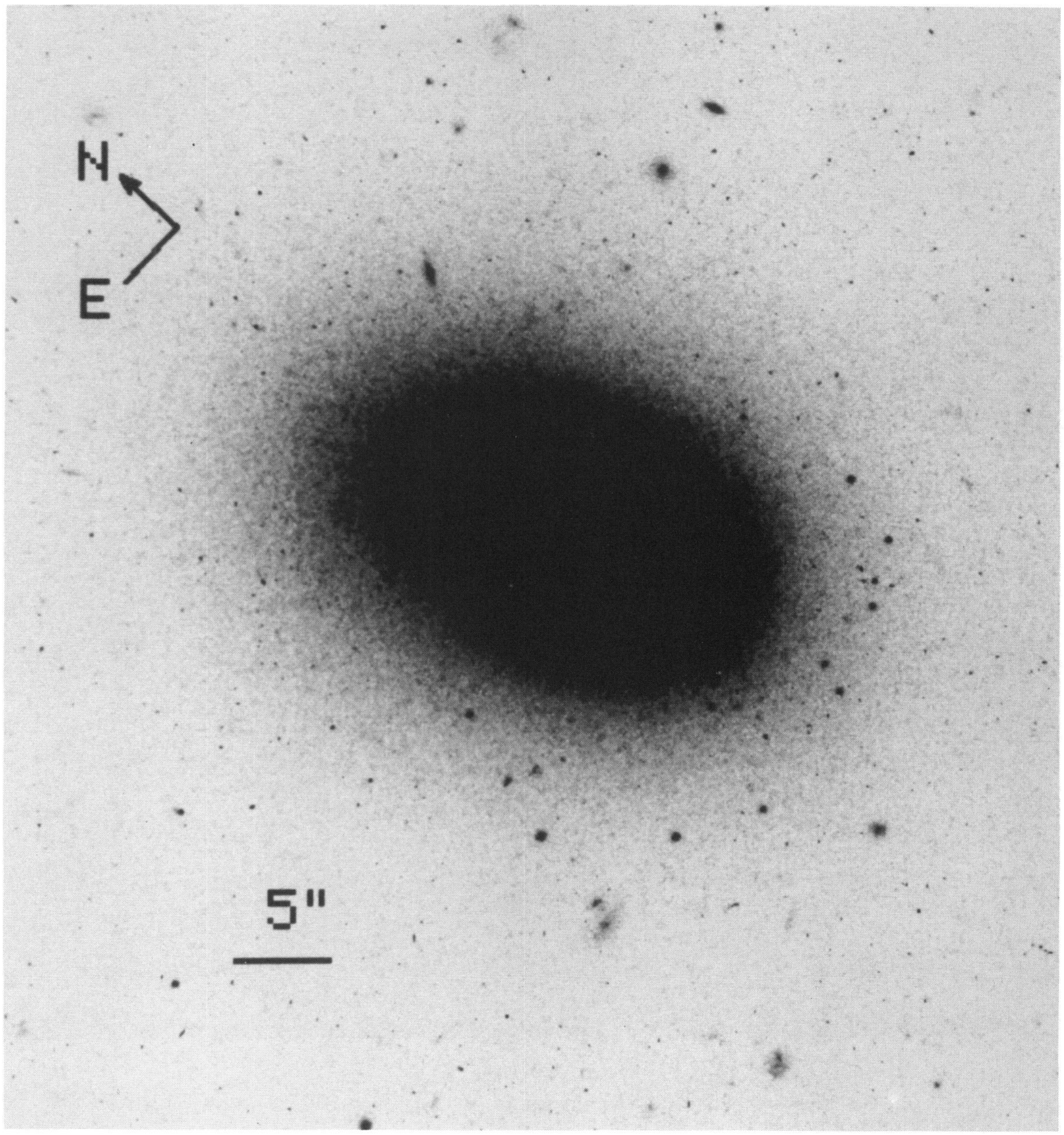

FIG. 1*b*

THUAN, IZOTOV, & LIPOVETSKY (see 463, 121)

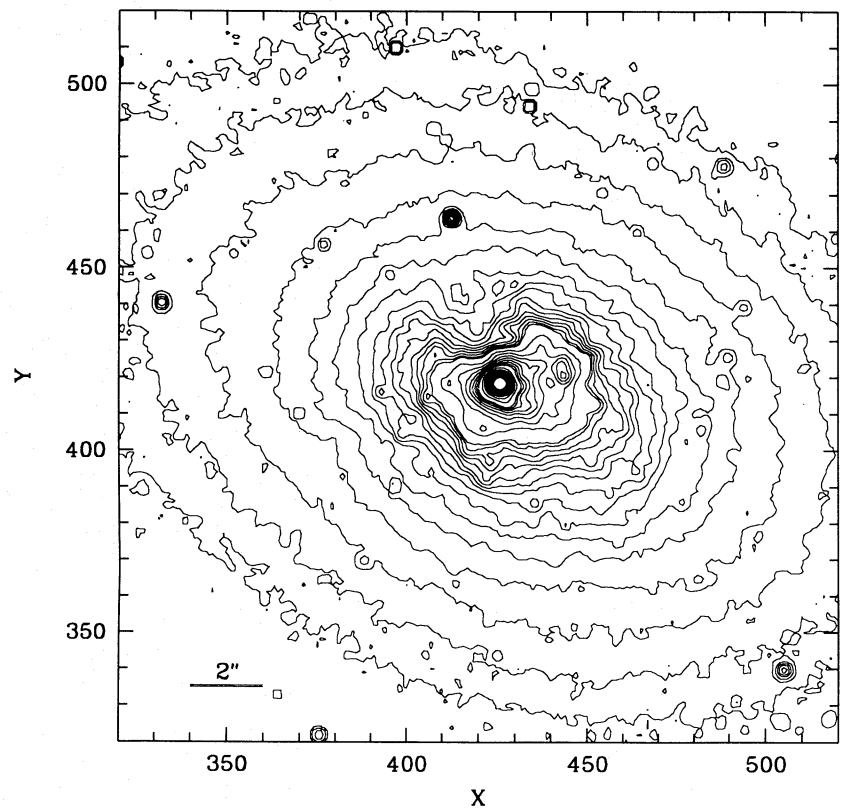

FIG. 2*a*

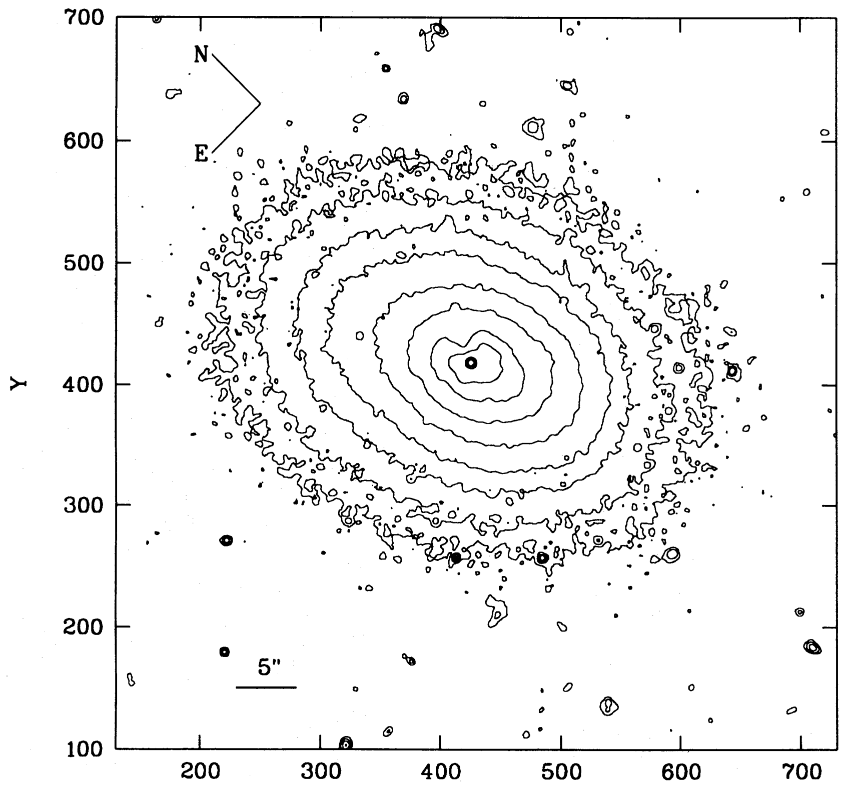

FIG. 2*b*

FIG. 2.—(*a*) Isophotal contour map of the inner part of Mrk 996. The second star-forming region to the west of the nuclear starburst and the deformation of the elliptical contours due to the dust patches north of the nucleus are clearly seen. The axes are labeled in pixels (1 pixel = 0″.102), and the *xy*-values given in Table 2 for the pointlike sources refer to this coordinate system. (*b*) Isophotal contour map of the outer part of Mrk 996. The pixel coordinate system is the same as in (*a*). It is clearly seen that the nuclear star-forming region is not at the center of the outermost isophote.

nuclear star-forming region is embedded in a lower surface brightness, elliptically shaped component. This morphology is relatively rare among BCDs. Loose & Thuan (1985) found that the vast majority of BCDs ($\geq 70\%$) belong to the iE BCD class, i.e., they possess an elliptically (E) shaped underlying low surface brightness component, although their star-forming activity is not nuclear but spread out in the central regions over several irregularly (i) shaped centers of star formation, within a region of ≤ 2 kpc in size. In contrast, only a minority ($\leq 20\%$) of BCDs belong to the nE BCD class, i.e., they have nuclear (n) star formation embedded in an elliptically shaped low surface brightness component. Evidently, Mrk 996 is of the nE type.

It is clearly seen from both Figure 1*b* and the isophotal map in Figure 2*b* that the nuclear star-forming region is *not* exactly at the center of the outermost isophote. There is a distinct asymmetry, the envelope being more extended to the northeast side than to the southwest side of the galaxy. Figure 1*b* also shows a swarm of pointlike sources to the south of the galaxy. Again, there is a distinct asymmetry in the spatial distribution of these pointlike sources: Nearly all of them are found in the south of the galaxy, while they are nearly absent to the north. The reason for this asymmetry is unclear. Mrk 996 shows no evidence of tidal interaction with a nearby companion galaxy. In fact, the BCD is rather isolated, having no projected companion within a $\sim 20'$ radius (corresponding to 126 kpc at the distance of Mrk 996). Perhaps the asymmetry is left over from a past merger.

3.2. *Surface Brightness and Color Distributions*

Surface photometry was done by fitting ellipses to the isophotal contours using the task ELLIPSE in STSDAS. We show in Figure 3 the V and I surface brightness distributions as a function of r, the equivalent radius of the best fitting elliptical isophote defined as $r = (ab)^{1/2}$, where a and b are the semimajor and semiminor axes of the ellipse, respectively. As the very central pixels are saturated, we show only the data for $r > 0''.13$ for the V profile and for $r > 0''.18$ for the I profile. The surface brightness profiles are plotted in three different two-parameter functional forms: (1) an exponential law characteristic of a disk structure $I = I_0 \exp(-\alpha r)$; (2) a power law $I = I_0 r^{-n}$; and (3) a de Vaucouleurs law characteristic of spheroidal components $\log I = \log I_e - 3.33[(r/r_e)^{1/4} - 1]$, where r_e is the effective radius containing half of the light of the model and I_e is the effective surface brightness at that radius.

Examination of Figure 3 reveals that both V and I surface brightness profiles can be fitted by an exponential law for $r \geq 8''$. There is a slight excess above the exponential fit in the radius range $3'' \leq r \leq 7''$, suggesting a faint bulge component in Mrk 996. The rise above the exponential law for $r \leq 3''$ is caused by the nuclear star-forming region, and the slight depression at $r \sim 2''$ is due to the dust patches discussed above. Both a power-law and a de Vaucouleurs–law profile do not provide a good fit to the outer parts because the V and I profiles drop below these fits at large radii ($r \geq 10''$). Thus, it is best to interpret the extended low surface brightness component as an exponential disk. This interpretation is reenforced by the fact that, beyond the nuclear star-forming and dusty regions ($r \geq 3''$), the ellipticity and position angles become constant, being equal to ~ 0.3 and $\sim 23°$ (as measured eastward from north), respectively. The best fits to the outer parts ($r \geq 8''$) of the V and I surface brightness distributions are given by

$$\mu_V = (20.00 \pm 0.18) + (0.270 \pm 0.020)r , \quad (3)$$

$$\mu_I = (19.11 \pm 0.13) + (0.269 \pm 0.015)r . \quad (4)$$

They are shown by the straight lines in Figure 3*a*. Equations (3) and (4) yield a scale length $\alpha_V^{-1} = \alpha_I^{-1} = 0.42$ kpc and a central surface brightness corrected for Galactic extinction ($A_V = 0.10$ mag and $A_I = 0.06$ mag, Burstein & Heiles 1982) $\mu_{V_0} = 19.90$ mag arcsec^{-2} and $\mu_{I_0} = 19.05$ mag arcsec^{-2}. With $(B-V) = 0.44$ (Izotov et al. 1993), then $\mu_{B_0} = 20.34$ mag arcsec^{-2} for Mrk 996. This is 1.3 mag arcsec^{-2} brighter than the value of 21.65 B mag arcsec^{-2} found by Freeman (1970) for spiral disks. The scale length of 0.42 kpc is among the 10% smallest scale lengths found for BCDs (Lipovetsky et al. 1995). Low surface brightness (LSB) dwarf spirals have been discussed by Schombert et al. (1995). These dwarf spirals have total blue luminosities

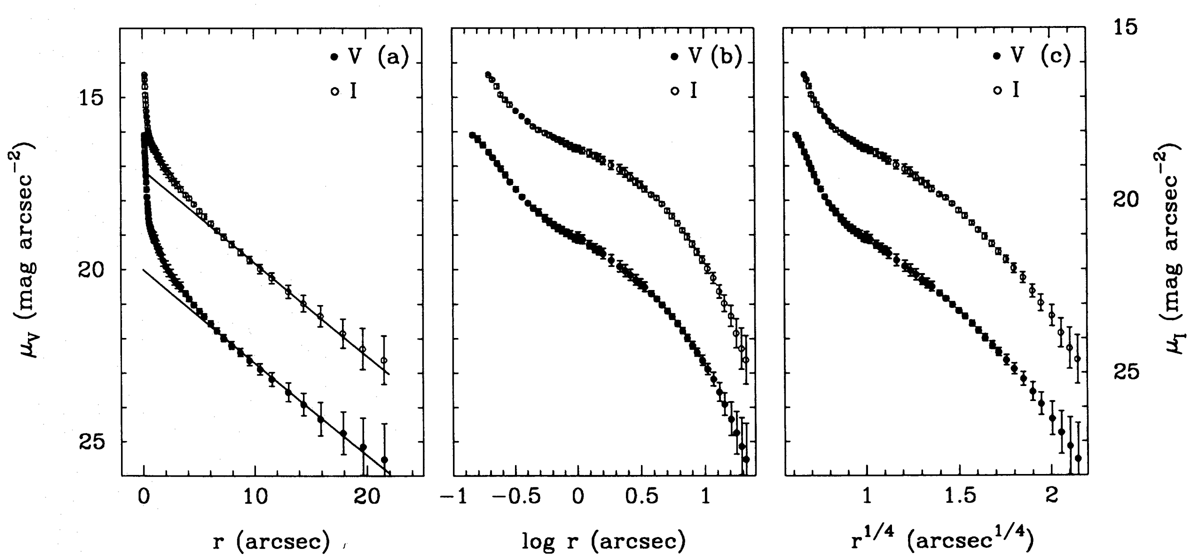

FIG. 3.—V and I surface brightness (in mag arcsec^{-2}) profiles as a function of the equivalent radius $r = (ab)^{1/2}$ in arcseconds, in three different two-parameter functional forms. In each case, a perfect fit would be a straight line. The three functional forms are (1) an exponential law that gives the best fit to the outer part of the galaxy, (2) a power law, and (3) a de Vaucouleurs $r^{1/4}$ law. The two latter laws overestimate the light at large radii ($r \geq 10''$). The error bars take into account photon statistics.

$M_B > -17$, comparable to that of Mrk 996, but their disk scale lengths are larger, varying between 1.1 and 2.8 kpc, and their central surface brightness are several magnitudes fainter ($\mu_{I_0} \geq 22$ mag arcsec^{-2}). Thus, the disk of Mrk 996 is not similar to those of LSB dwarf spirals, and Mrk 996 cannot simply be thought of as a LSB dwarf spiral undergoing a nuclear burst of star formation.

Mrk 996 does not resemble other dwarf spirals in other aspects. The galaxy does not show obvious spiral structure in the disk (Figs. 1*a* and 2). The only hint of a possible two-arm spiral-like structure is best seen in the $(V-I)$ color map (Fig. 4*a*, [Pl. 12], is a gray-scale representation, while Fig. 4*b*, [Pl. 13], is a contour map), where the spiral-like pattern, which is connected to the nuclear star-forming region, is confined to a region no larger than 1."5 (160 pc) in radius. To put in evidence features with smaller contrast, we have subtracted the surface formed by the elliptical fits used to derive the surface brightness profile from the V image. The result is shown in Figure 5 (Plate 14). Again, the east-west spiral-like structure can be seen. Although we cannot rule out the interpretation that the spiral shape is merely the accidental result of the interplay between the geometries of the star formation and dust obscuration zones, we suspect the spiral-like structure to be real because a blue star-forming region, at ~200 pc from the nucleus, is associated with the western arm. If this is true, the very existence of such a spiral feature confined to the very inner part of the disk of a dwarf galaxy poses interesting challenges to theories of formation of such structures in dwarf galaxies.

The color map also shows that the blue central star-forming region is divided into at least two subregions: the nucleus and another star-forming region at ~0."5 (50 pc) south of the nucleus. Figure 6 shows the $V-I$ color profile of Mrk 996. The very blue color at the center (at $r \sim 0.''2$, $V-I \sim 0.15$) is due to the star-forming region. The galaxy becomes gradually redder with increasing r reaching a constant $V-I \sim 0.9$ at $r \geq 4''$. This red color is that of the underlying low surface brightness component and corresponds roughly to that of a K1 main sequence or G5 giant star. We have used here the color spectral–type calibration of Bessell (1990), which holds for stars with solar metallicity. For stars with 1/10 of the Sun's metallicity, as in Mrk 996 (see below), the corresponding spectral types at a given $(V-I)$ color are slightly later. The V_{25} isophotal diameter at the surface brightness level of 25 mag arcsec^{-2} is 37", corresponding to a linear diameter of 3.9 kpc. Total magnitudes corrected for Galactic extinction are $V = 14.52 \pm 0.01$ mag and $I = 13.77 \pm 0.01$ mag.

Neutral hydrogen has been detected in Mrk 996 by Thuan et al. (1995). The detected H I emission feature has a central heliocentric velocity $v_{\rm H\,I} = 1622 \pm 10$ km s^{-1}, full velocity widths at 20% and 50% of peak intensity $\Delta v_{20} = 177 \pm 25$ km s^{-1} and $\Delta v_{50} = 83 \pm 25$ km s^{-1}, and a H I flux of 1.04 ± 0.16 Jy km s^{-1}, corresponding to a H I mass of 1.1×10^8 $M_\odot$. We calculate an indicative total mass $M_T = 4.3 \times 10^8$ $M_\odot$, following Thuan & Martin (1981) and taking d_{25}, the galaxy diameter at a blue surface brightness level of 25 mag arcsec^{-2}, to be 35". This gives $M_{\rm H\,I}/M_T = 0.26$. With $L_B = 9.7 \times 10^8$ $L_{B\odot}$, we derive $M_{\rm H\,I}/L_B = 0.12$ and $M_T/L_B = 0.44$. These ratios are not unusual for BCDs (Thuan & Martin 1981).

We note that the photometric structure of Mrk 996 is somewhat different from that of the prototype nE BCD Haro 2 studied by Loose & Thuan (1986). These authors found that the light profile of the low surface brightness component in Haro 2 is best fitted not by an exponential law, like in the case of Mrk 996, but by a power law, not unlike the light profile of dwarf elliptical galaxies. They suggested that Haro 2 is an extreme example of a dwarf elliptical with neutral hydrogen and very active star formation at its center. The nE BCD class thus appears to contain both disk and elliptical galaxies.

3.3. *Photometry of Pointlike Sources*

Projected against and around the galaxy, there can be seen many (~40) pointlike sources (FWHM ~ 0."2). We

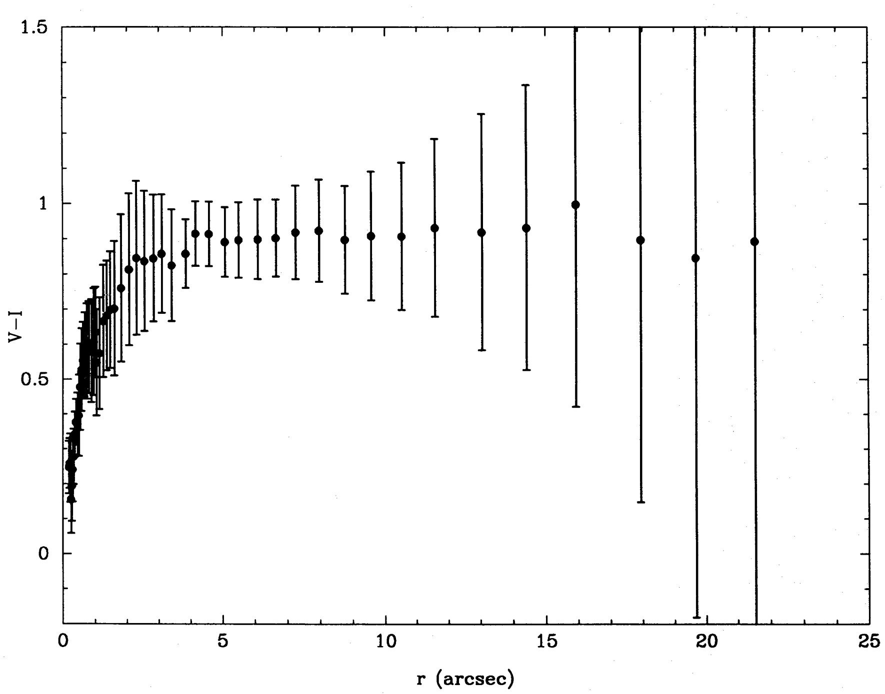

FIG. 6.—The $V-I$ color profile of Mrk 996. The error bars take into account photon statistics.

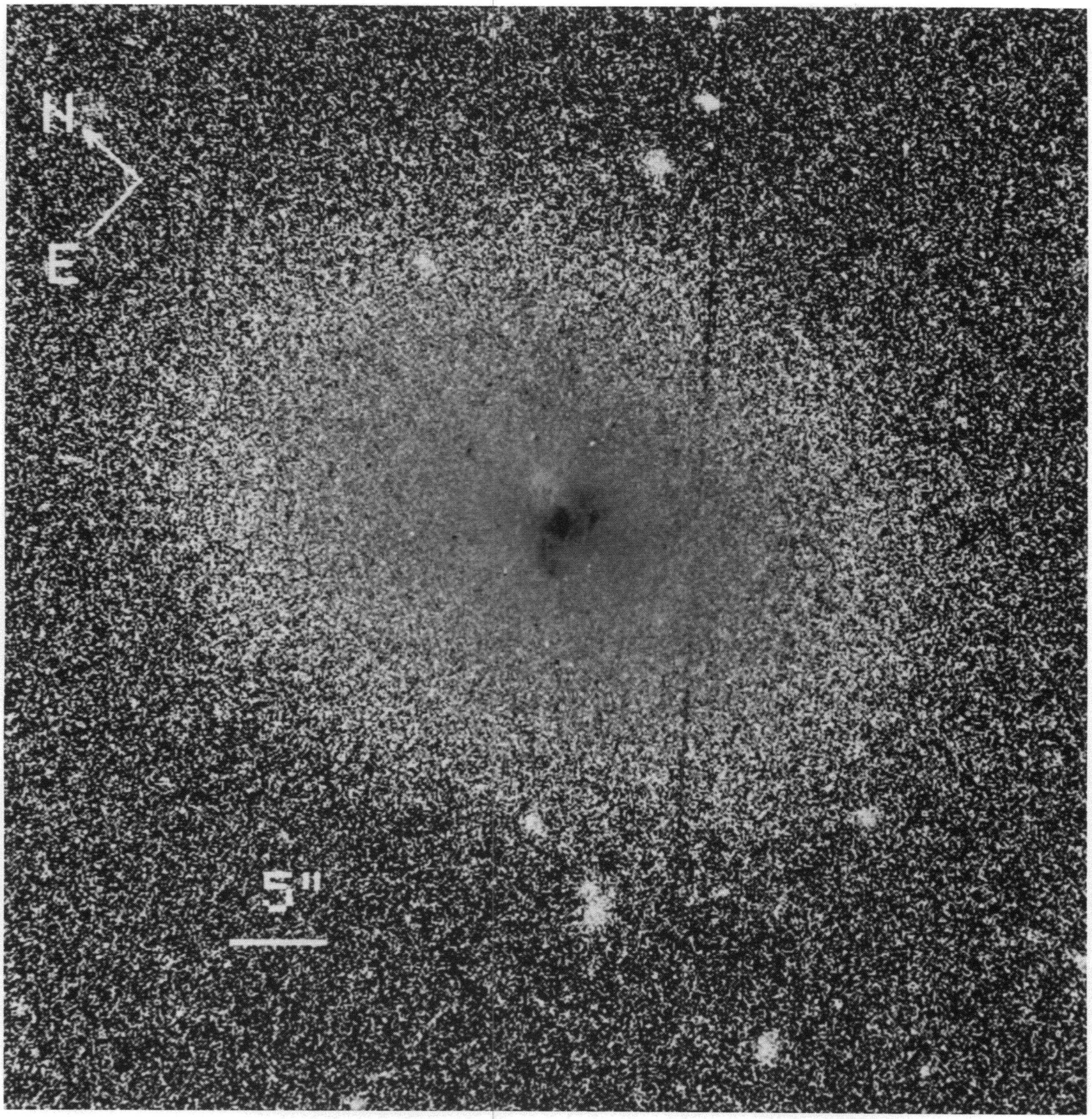

FIG. 4a

FIG. 4.—(a) $(V-I)$ gray-scale color map. A two-arm spiral-like stucture is seen within the inner 160 pc in radius. The dust patches to the north of the nucleus are clearly visible. The star-forming region to the west of the nucleus is on the western spiral arm. (b) Isophotal contour map of (a). The xy-axes are labeled in pixels (1 pixel = 0".102), and the coordinate system is the same as in Fig. 2.

THUAN, IZOTOV, & LIPOVETSKY (see 463, 124)

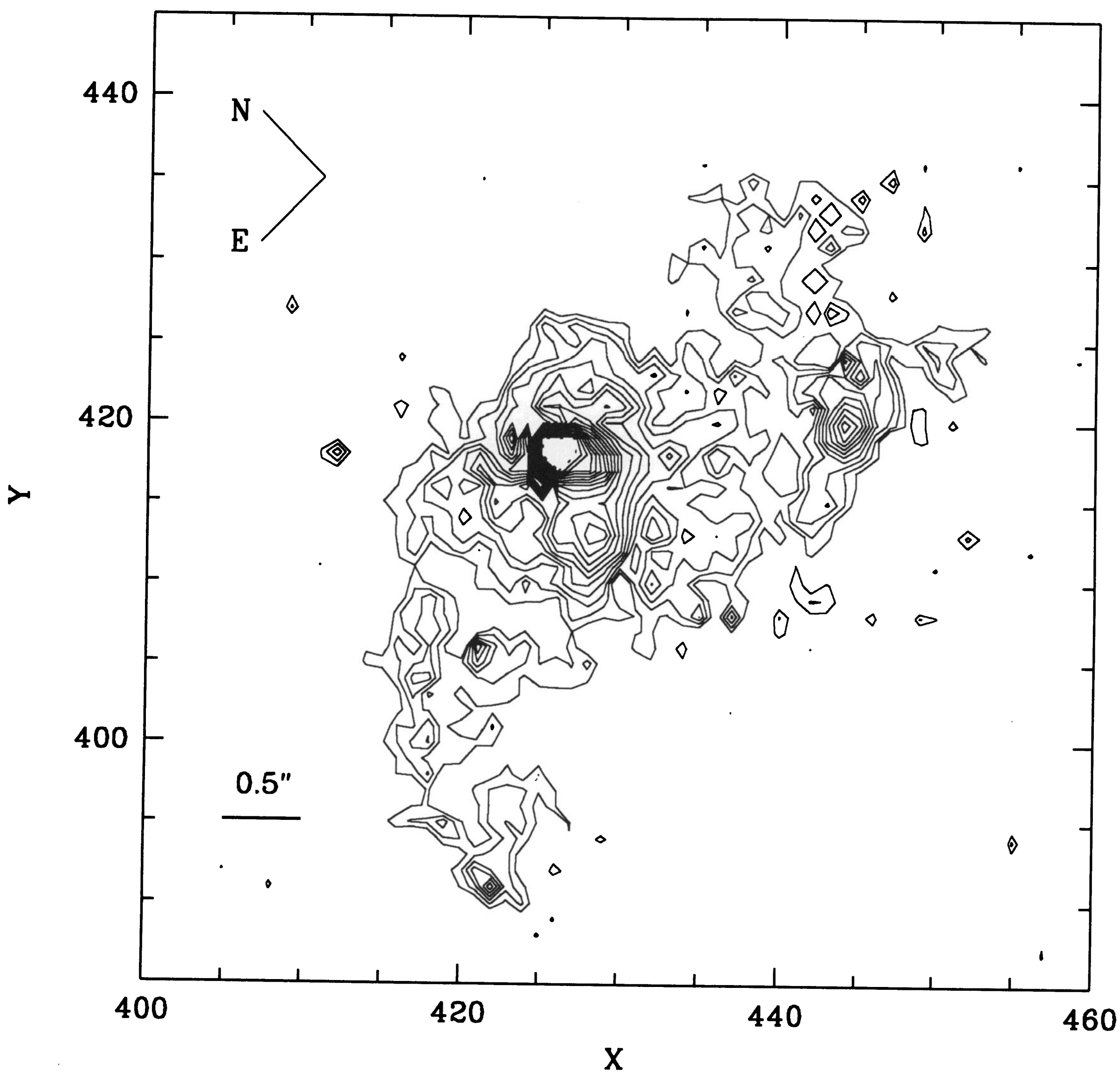

FIG. 4*b*

THUAN, IZOTOV, & LIPOVETSKY (see 463, 124)

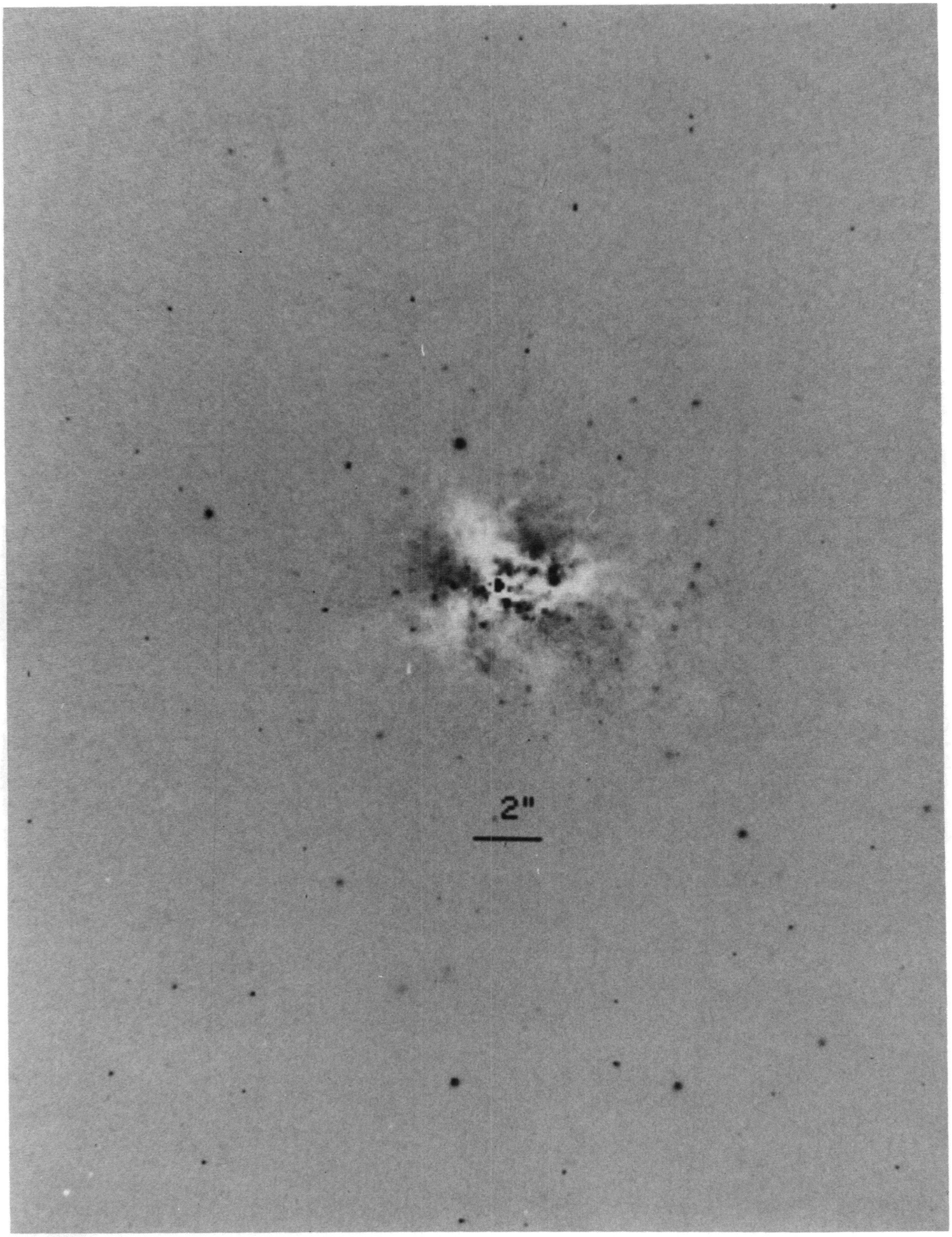

FIG. 5.—Difference between the V image and the surface formed by the elliptical fits used to derive the surface brightness profile. The orientation is the same as in Fig. 4a.

THUAN, IZOTOV, & LIPOVETSKY (see 463, 124)

have already mentioned the swarm of stellar sources to the southside of the galaxy (Fig. 1*b*). Around the nuclear star-forming region, many stellar sources can also be distinguished (Fig. 1*a*). We have measured the V and I magnitudes and $(V-I)$ colors of all point sources with $V \leq 24$ mag and listed them along with their errors in Table 2. Aperture photometry of the pointlike objects was performed using the package APPHOT in IRAF. Good results were obtained using a circular aperture of radius 5 pixels for the objects and, for the background, a surrounding annulus covering 2–4 pixels for objects near the star-forming zone, and 5 pixels for objects outside the galaxy. The x and y coordinates given in Table 2 refer to the coordinate system defined in Figure 2. The photometry of the inner clusters is less precise because of the bright background. The magnitudes and colors have been corrected for foreground extinction. The internal extinction derived from spectrophotometry for the nuclear region is larger, $A_V - A_I = 0.45$, corresponding to $E(B-V) = 0.36$ (see § 3.4), but since we do not know whether the pointlike sources near the nuclear star-forming region are foreground sources seen in projection near the center or whether they are physically associated with the star-forming region, we have chosen not to correct them for internal extinction.

Figure 7 shows that the magnitudes of most of the point sources vary between $I_0 = 21$ and $I_0 = 24$ mag, corresponding to absolute magnitudes M_{I_0} between -10.7 and -7.7. It also shows that the pointlike sources have a remarkably small dispersion in the $(V-I)_0$ color. The vast majority of the points have $(V-I)_0$ colors between 0.7 and 1.1, with a mean of ~ 0.9; a color range that matches those found for globular clusters such as ω Cen or NGC 6752 (Harris et al. 1993). The interpretation that the vast majority of the pointlike sources are globular clusters with ages $\geq 10^{10}$ yr is reenforced by their visual absolute magnitude range ($-10.4 \leq M_V \leq -6.6$) and their diameters (≤ 20 pc). There are a few objects with $(V-I)_0$ colors very different from the mean. The bluest object in Table 2, No. 40, has a $(V-I)_0$ corrected for foreground extinction of ~ 0, similar to the color of the nuclear region (Fig. 6). Examination of

TABLE 2

MAGNITUDES AND COLORS OF POINTLIKE SOURCES

No.	x^a	y^a	V_0^b	I_0^b	$(V-I)_0^b$
1	221.00	180.00	23.295± 0.072	22.471± 0.044	0.824± 0.084
2	323.00	287.00	24.403± 0.136	23.241± 0.074	1.163± 0.155
3	413.50	257.50	23.164± 0.063	21.089± 0.022	2.075± 0.067
4	396.00	287.00	24.291± 0.140	23.294± 0.081	0.997± 0.162
5	411.00	294.00	24.312± 0.145	23.626± 0.107	0.686± 0.180
6	375.50	322.00	23.966± 0.113	23.101± 0.076	0.865± 0.136
7	485.00	257.00	23.138± 0.066	22.194± 0.038	0.943± 0.076
8	531.50	271.50	24.043± 0.112	22.939± 0.063	1.104± 0.129
9	518.00	326.50	24.963± 0.276	23.942± 0.202	1.021± 0.342
10	505.00	340.00	23.017± 0.074	22.092± 0.052	0.925± 0.090
11	572.50	334.00	23.875± 0.104	22.958± 0.064	0.916± 0.122
12	564.00	349.00	23.903± 0.106	23.127± 0.072	0.775± 0.128
13	590.00	379.00	23.867± 0.101	22.908± 0.065	0.959± 0.120
14	591.00	393.00	24.581± 0.167	23.559± 0.098	1.022± 0.194
15	599.00	415.00	23.930± 0.106	22.924± 0.062	1.006± 0.123
16	578.50	447.00	23.647± 0.088	22.634± 0.052	1.013± 0.102
17	488.50	478.00	23.771± 0.129	22.901± 0.098	0.871± 0.162
18	469.00	479.00	24.599± 0.242	23.472± 0.154	1.127± 0.287
19	455.00	471.00	23.770± 0.202	22.980± 0.180	0.790± 0.271
20	413.00	464.00	22.032± 0.053	21.070± 0.045	0.962± 0.070
21	417.00	481.00	24.852± 0.308	23.900± 0.260	0.952± 0.403
22	377.00	456.50	23.974± 0.192	23.703± 0.322	0.271± 0.375
23	332.00	440.50	23.248± 0.083	22.289± 0.052	0.959± 0.098
24	494.00	439.00	23.549± 0.165	22.761± 0.173	0.788± 0.239
25	490.00	426.00	23.748± 0.255	23.629± 0.342	0.119± 0.427
26	488.00	420.00	24.084± 0.259	23.258± 0.204	0.826± 0.330
27	482.00	406.00	23.596± 0.178	22.997± 0.236	0.600± 0.296
28	481.00	365.00	24.096± 0.166	22.282± 0.079	1.814± 0.184
29	441.00	370.00	23.959± 0.270	23.252± 0.257	0.707± 0.373
30	444.00	378.00	23.899± 0.363	23.014± 0.234	0.885± 0.432
31	436.00	385.00	24.097± 0.446	22.225± 0.200	1.872± 0.489
32	427.00	381.00	23.847± 0.337	23.006± 0.335	0.840± 0.475
33	388.00	370.00	24.007± 0.167	23.316± 0.155	0.691± 0.228
34	398.00	404.00	22.843± 0.216	21.820± 0.183	1.023± 0.283
35	393.25	416.00	23.031± 0.258	22.493± 0.295	0.538± 0.392
36	405.00	415.00	22.325± 0.254	21.287± 0.200	1.038± 0.323
37	395.50	448.50	23.799± 0.243	23.019± 0.276	0.780± 0.368
38	411.00	418.00	21.910± 0.106	21.193± 0.075	0.717± 0.130
39	421.00	406.00	22.275± 0.359	21.188± 0.231	1.087± 0.427
40	444.00	420.00	21.487± 0.168	21.536± 0.213	-0.049± 0.271
41	443.25	424.25	21.322± 0.171	20.596± 0.134	0.726± 0.217

[a] The coordinate system is shown in Fig. 2.
[b] Corrected for foreground extinction.

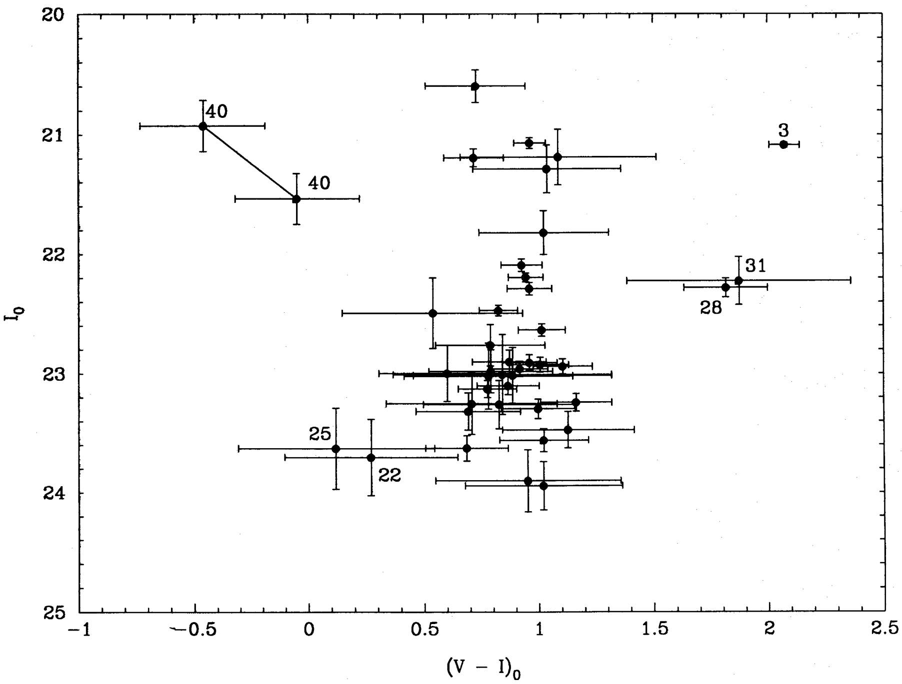

FIG. 7.—Color-magnitude diagram for the pointlike objects projected against and around Mrk 996. Magnitudes and colors have been corrected for foreground extinction. Most of the objects have $0.7 \leq (V-I)_0 \leq 1.1$, with a mean of ~ 0.9. The deviant points, labeled by their number in Table 2, are discussed in the text.

Figures 4*a* and 4*b* shows it to lie on the western spiral-like feature, so that its association with the nuclear star-forming region is probable. Correcting for the same internal extinction as the nuclear region gives $(V-I)_0 \sim -0.46$. In Figure 7 we have shown object 40, both with and without internal extinction, as two points connected by a line. The true situation is probably intermediate between these two points. In any case, the range of $(V-I)_0$ colors spanned is similar to that of young OB stars in star clusters like R136 in the LMC (Holtzman et al. 1995), so that object 40 is very likely a young star cluster. Objects 22 and 25 also have $(V-I)_0$ colors bluer than the mean. Taken at face value, they have $V-I$ colors of A main sequence of A and F supergiant stars (Bessell 1990), although the large color errors do not preclude these objects from being globular clusters. Objects 3, 28, and 31 have $(V-I)_0$ colors redder than average, corresponding to colors of foreground or background M main sequence or giant stars (Bessell 1990).

We have plotted in Figure 8 the number of globular clusters per 0.5 mag bin for all objects listed in Table 2, except for objects 3, 28, 31, and 40. For $-9 \leq M_V \leq -7.5$, the shape of the globular cluster luminosity function in Mrk 996 is remarkably similar to that in the Milky Way (Harris 1991). Our data become incomplete for $M_V \geq -7.5$. At the bright end ($M_V \leq -9$), there appears to be more clusters in Mrk 996 than in the Milky Way, with a brighter magnitude cutoff in Mrk 996. The brightest globular cluster in Mrk 996 has $M_V \sim -10.4$, as compared to $M_V \sim -9.5$ for the brightest one in the Milky Way.

3.4. *Spectrophotometry of the Nuclear Region*

The UV and optical spectra of the inner 45 pc in radius of the nuclear region of Mrk 996 are shown in Figure 9, with the identification of each detected line. The observed line intensities are given in Table 3. The spectra are characterized by several unusual features, suggestive of extraordinary physical conditions. In the UV range, the N III] λ1750 line is particularly intense, much more intense than in other emission-line dwarf galaxies. Garnett et al. (1995) obtained spectra of seven such objects with the FOS and found that the N III] λ1750 line is only present in the H II region N88A in the SMC at a very weak level. On the other hand, the O III] λ1663 emission line in Mrk 996 is weaker than in the Garnett et al. (1995) objects. Another striking feature of the UV spectrum is the unusually large width (FWHM $\sim$ 900 km s^{-1}) of the N III] λ1750 line as compared with that of the Si III] λ1895 and C III] λ1909 lines (FWHM $\leq$ 600 km s^{-1}). The optical spectrum exhibits the unusual properties already discussed in the introduction: large He I λ4471, λ5876, and λ6678 line intensities and emission lines of high-ionization stages being broader than those of low-ionization stages. There are strong, broad Wolf-Rayet bumps at λ4640 and λ4686, suggesting the presence of a large WN stellar population, and also a C IV bump at λ5808, indicative of WC stars.

There are also a number of lines whose intensities are unusually large or are not ordinarily seen in H II region spectra. The auroral lines [N II] λ5755 and [O III] λ4363 are very intense. The He I λ4144 and λ5048 lines, which are not ordinarily seen, are present and so are the [Fe II] λ4243, λ4287, and λ5158 lines, which are seen in supernova remnant spectra and are attributed to shock excitation (Danziger 1983) but are not usually seen in H II region spectra. The [Fe IV] λ5233 and O II λ4417 lines are also present. The presence of these unusual lines could be due to the very high electron density in the nuclear star-forming region, as discussed later. We note that many of the emission lines seen in Mrk 996 are often observed in spectra of young planetary nebulae and symbiotic stars, with similar values of electron temperature and density (Lutz et al. 1989; Feibelman, Aller, & Hyung 1992; Hyung, Aller, & Feibelman 1994).

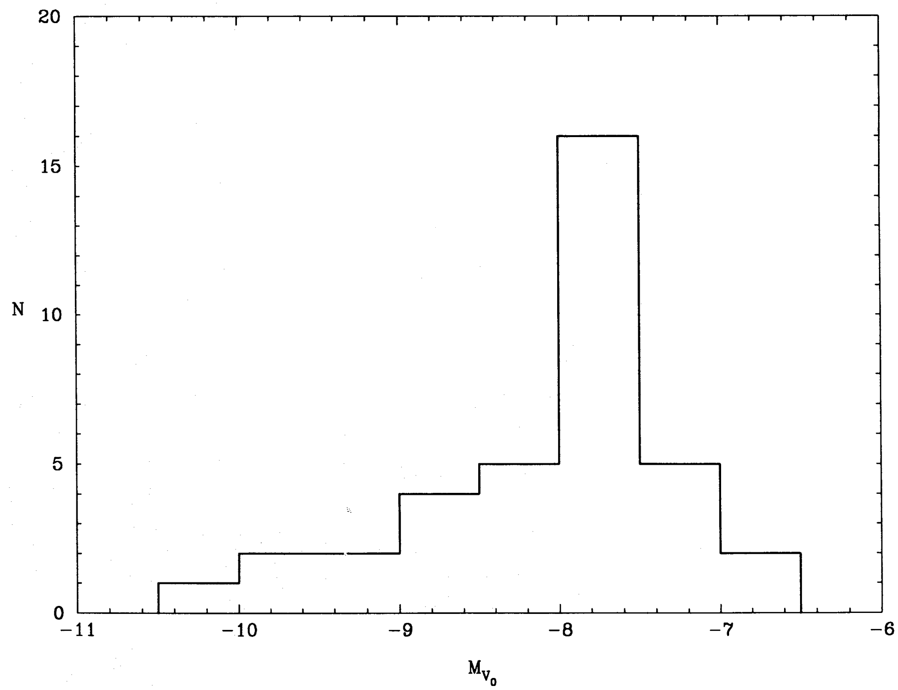

FIG. 8.—The luminosity function of globular clusters in Mrk 996. The clusters labeled 3, 28, 31, and 40 in Fig. 7 have been excluded. The absolute magnitudes M_{V_0} have been corrected for foreground extinction.

The line intensities corrected for extinction are also given in Table 3. The hydrogen lines have also been corrected for underlying absorption following Izotov et al. (1994). The errors listed for the corrected line intensities also take into account the errors in the emission-line equivalent widths. We have used the extinction curve derived for the SMC in the UV range (Rocca-Volmerange et al. 1981) and that derived by Whitford (1958) in the optical range. The derived extinction coefficient is high, $C(\mathrm{H}\beta) = 0.53$ dex, corresponding to $E(B-V) = 0.36$ mag and $A_V = 1.11$ mag. It was taken to be the mean of the extinction coefficients derived from the $F(\mathrm{H}\alpha)/F(\mathrm{H}\beta)$, $F(\mathrm{H}\gamma)/F(\mathrm{H}\beta)$, and $F(\mathrm{H}\delta)/F(\mathrm{H}\beta)$ ratios weighted by the intensities of the Hα, Hβ and Hδ lines. An unweighted mean would have given a slightly smaller extinction coefficient $C(\mathrm{H}\beta) = 0.43$ dex. Another estimate of the extinction coefficient can be obtained from the [O III] λ4363/O III] λ1663 intensity ratio, which depends only on the effective temperature T_e and $C(\mathrm{H}\beta)$. Adopting $T_e = 15{,}000$ K as given by H II region models (see later), $C(\mathrm{H}\beta) = 0.34 \pm 0.13$ dex if the SMC UV extinction curve (Rocca-Volmerange et al. 1981) is used, and $C(\mathrm{H}\beta) = 0.48 \pm 0.18$ dex if the Galactic UV extinction curve (Seaton 1979) is used (Peimbert 1995). These values are not very different from the one derived from the Balmer lines. We adopt the latter because the O III] λ1663 is very weak and not very well measured (see the UV spectrum in Fig. 9). The derived high extinction is not surprising given the dust patches clearly seen in Figure 1*a*. Adopting the same extinction coefficient in the UV range would lead to unrealistically large UV line intensities. However, Fanelli, O'Connell, & Thuan (1988) have found that, in blue compact galaxies, the amount of UV extinction is significantly smaller than values derived from the Balmer decrement. Because dust is efficiently destroyed or removed from the vicinity of O stars by the combined action of ionizing radiation, stellar winds, and supernovae, the UV light preferentially emerges through windows of low-optical depth. Fanelli et al. (1988) found the relation $E(B-V)_{\mathrm{UV}} \sim E(B-V)_{\mathrm{Balmer}} - 0.3$ mag, which we adopt here. This gives $C(\mathrm{H}\beta) = 0.09$ for the UV lines.

To derive ionic and element abundances in giant H II regions, it is customary to adopt a low-density ($N_e \sim 100$ cm^{-3}) ionization-bounded two-zone H II region model (see, for example, Izotov et al. 1994). However, this simple model cannot be applied to the nuclear star-forming region of Mrk 996 for several reasons. First, the electron temperature derived from the [O III] λ4363/(λ4959 + λ5007) line intensity ratio would be unrealistically high, exceeding 30,000 K. Ionized gas heated beyond $\sim$20,000 K would cool down very fast due to hydrogen cooling. Second, this would lead to unrealistic heavy-element abundance ratios. Third, the helium abundance derived, $Y \geq 0.3$, would be unphysically large. Blue compact galaxies have $Y \leq 0.27$ (Izotov et al. 1994). Thus, we do not believe the very low oxygen abundance derived for Mrk 996 in the context of this model, about 1/40 that of the Sun, to be correct.

We argue instead that a high-density ($N_e \geq 10^6$ cm^{-3}) compact H II region model with outflow motions is much more appropriate for Mrk 996. A high electron density is required to explain the very low intensity of the line blend He I + H8 λ3889. The intensity of this blend is expected to be $\sim$20% of the Hβ intensity when corrected for extinction, with roughly equal contributions from the hydrogen and helium lines. The observed blend intensity corrected for extinction is only $\sim$13% (Table 3). A plausible explanation is a very high density medium where the He I λ3889 line (but not the H8 line) would be optically thick and substantially reduced in intensity. A very high density would also naturally yield a lower temperature ($\lesssim$20,000 K) as derived from the [O III] λ4363/(λ4959 + λ5007) line ratio. Moreover, such a high electron density is suggested by the very morphology of the galaxy (Fig. 1). As discussed in § 3.1, all the star-forming activity in Mrk 996 is confined to an extremely compact nuclear region of radius $\sim$315 pc. Finally,

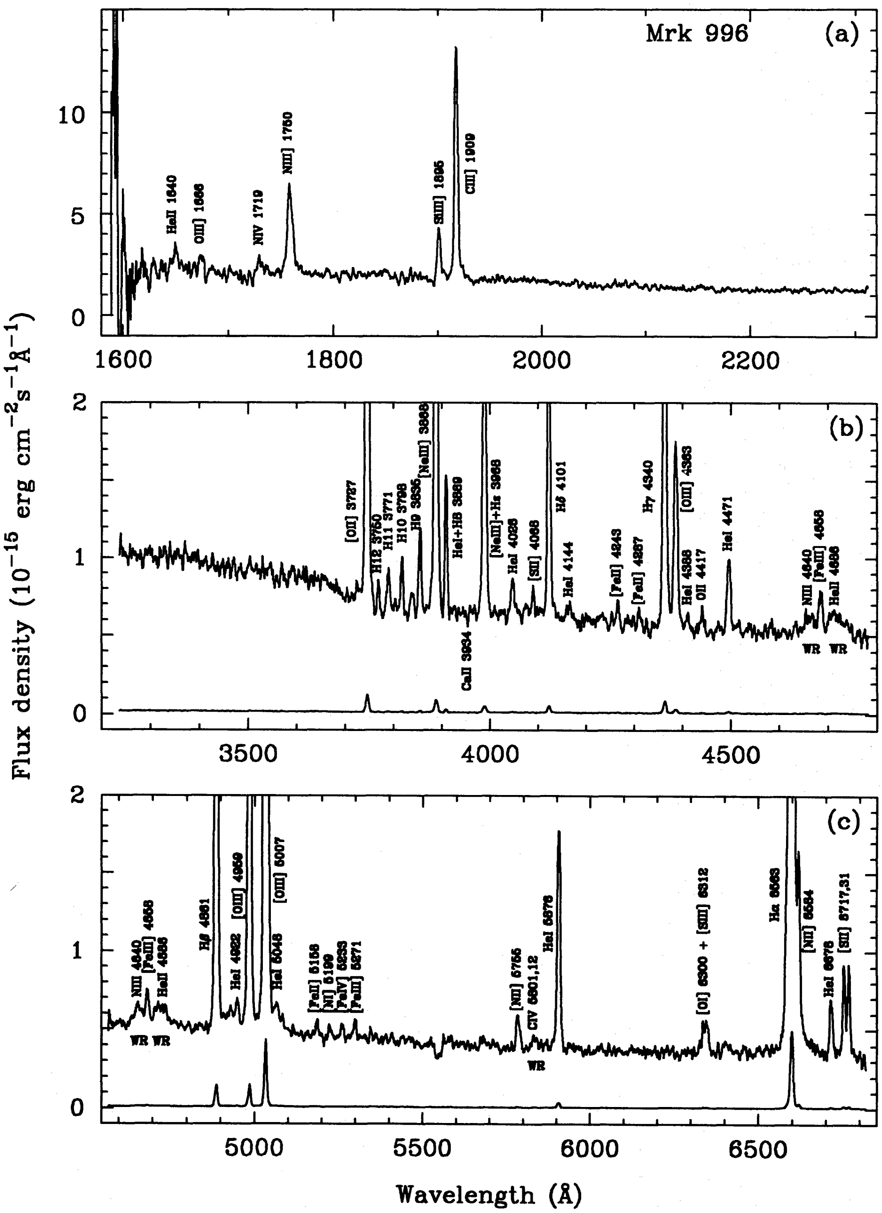

FIG. 9.—(*a*) *HST* UV FOS spectrum, (*b*) *HST* blue FOS spectrum, and (*c*) *HST* red FOS spectrum. All spectra were taken with a 0ʺ86 circular aperture giving a spectral resolution of ~3 Å for the UV spectrum, ~6 Å for the blue spectrum and ~9 Å for the red one. Identification for the emission lines are given.

assuming a high electron number density may help to solve the problem of the unrealistic values of the He and heavy-element abundances. We also need to account for the fact that the high-excitation forbidden and helium lines are broader than the low-excitation lines. A natural model would be a H II region not in hydrostatic equilibrium, but whose high-excitation zones are expanding with a velocity of ~ 500 km s^{-1}, a value derived from the width of the N III] $\lambda 1750$ UV line (Fig. 9*a*). This expansion motion can be caused by Wolf-Rayet stellar winds and/or supernovae.

H II region models were constructed with the radiative-collisional equilibrium program CLOUDY (Ferland 1993). The following input parameters have to be specified for each model. They are Q(H), the logarithm of the number of ionizing photons per second, and $T_{\rm eff}$, the effective temperature of the ionizing stars. The inner radius $r_{\rm in}$ was chosen to be 1 pc to take into account the finite size of the ionizing star cluster ($r_{\rm in} = 0$ would correspond to a point ionizing source). We failed to find ionization-bounded H II region models that could reproduce satisfactorily at the same time the observed low- and high-excitation line intensities, so we shall discuss here only density-bounded H II region models. These models require an additional input parameter that is the outer radius $r_{\rm out}$, beyond which the electron number density drops to zero. The radial dependence of the electron number density also needs to be specified. In the context of a two-zone model, we adopt for the inner high-excitation zone a central density N_0 and a radial power-law dependence $N_e \propto r^{-\alpha}$, where $\alpha = 2$. The slope 2 corresponds to the case of a gas expanding with constant velocity. Farther out, when density drops to $N_1 \sim 450$ cm^{-3}, roughly the value derived from the [S II] $\lambda 6717/\lambda 6731$ ratio, we adopt a constant density for the low-excitation region equal to N_1, out to $r_{\rm out}$. The remaining input parameters are the filling factor f and the helium and heavy-element (C, N, O, Ne, Si, S, and Fe) abundances rela-

TABLE 3

UV AND OPTICAL EMISSION LINE INTENSITIES

Ion	Observations		Models	
	F(λ)/F(Hβ)	I(λ)/I(Hβ)[a]	I	II
1663 O III]	0.070±0.030	0.110±0.047	0.277	0.246
1750 N III]	0.436±0.030	0.685±0.047	0.123	0.678
1895 Si III]	0.182±0.019	0.286±0.030	0.251	0.204
1909 C III]	0.720±0.030	1.130±0.047	1.231	1.110
3727 [O II]	0.635±0.030	0.922±0.046	0.920	0.814
3750 H12	0.020±0.006	0.034±0.017	...	...
3771 H11	0.029±0.009	0.046±0.021	...	...
3798 H10	0.035±0.009	0.054±0.020	...	...
3835 H9	0.056±0.009	0.083±0.020	...	...
3868 [Ne III]	0.486±0.027	0.670±0.038	0.650	0.637
3889 He I + H8	0.090±0.010	0.128±0.020	0.200	0.190
3968 [Ne III]+H7	0.268±0.021	0.361±0.031	0.350	0.345
4026 He I	0.028±0.009	0.036±0.012	...	...
4068 [S II]	0.013±0.005	0.017±0.006	0.017	0.015
4101 Hδ	0.226±0.019	0.291±0.028	0.293	0.294
4340 Hγ	0.419±0.025	0.494±0.031	0.501	0.502
4363 [O III]	0.176±0.019	0.205±0.022	0.219	0.206
4471 He I	0.063±0.022	0.071±0.025	0.040	0.040
4640 N III	0.051±0.017	0.055±0.018	...	...
4658 [Fe III]	0.038±0.014	0.040±0.015	0.042	0.037
4686 He II	0.079±0.014	0.083±0.015	...	...
4861 Hβ	1.000±0.031	1.000±0.032	1.000	1.000
4922 He I	0.022±0.006	0.021±0.006	...	...
4959 [O III]	0.961±0.029	0.932±0.029	0.918	0.908
5007 [O III]	2.863±0.070	2.739±0.068	2.753	2.723
5158 [Fe II]	0.015±0.005	0.013±0.005	...	...
5199 [N I]	0.013±0.002	0.012±0.001	...	...
5233 [Fe IV]	0.013±0.005	0.012±0.005	...	...
5271 [Fe III]	0.017±0.005	0.015±0.005	0.024	0.021
5755 [N II]	0.044±0.008	0.035±0.006	0.007	0.039
5808 C IV	0.020±0.007	0.015±0.006	...	...
5876 He I	0.256±0.014	0.197±0.011	0.144	0.142
6300 [O I]	0.025±0.004	0.017±0.003	0.002	0.002
6312 [S III]	0.036±0.009	0.025±0.007	0.056	0.050
6563 Hα	4.215±0.100	2.804±0.073	2.793	2.779
6584 [N II]	0.239±0.015	0.158±0.010	0.147	0.894
6678 He I	0.060±0.009	0.039±0.006	...	...
6717 [S II]	0.083±0.007	0.053±0.004	0.047	0.042
6731 [S II]	0.082±0.007	0.053±0.004	0.045	0.040
C(Hβ) dex	0.53			
F(Hβ)[b]×10[13] erg s^{-1}cm^{-2}	2.2			
log L(Hβ)[b] erg s^{-1}	40.09		40.09	40.11
EW(Hβ) Å	129			
EW(abs) Å	0.3			

[a] Line intensities were corrected using $C(H\beta) = 0.09$ for UV lines and $C(H\beta) = 0.53$ for optical lines.

[b] Corrected for extinction.

tive to hydrogen. For all elements except nitrogen, we adopt element abundance ratios with respect to oxygen close to those observed in low-metallicity BCDs (Thuan et al. 1995; Garnett et al. 1995).

Using CLOUDY, we have run a series of models varying the input parameters to search for those models that give line intensities closest to the observed ones and yield the correct total dereddened Hβ luminosity of 1.23×10^{40} ergs s^{-1} (Table 3). The input parameters of the two best models are given in Table 4. The parameters are very nearly the same in the two models, except for the nitrogen abundance, which is ~6 times higher in model 2 than in model 1. In both models, $r_{in} = 1$ pc and $r_{out} = 300$ pc. The last value approximates well the size of the nuclear star-forming region in Mrk 996 (Fig. 1). This would give a transition radius of ~100 pc between the high- and low-excitation zones. The best value for the filling factor, $f = 2.6 \times 10^{-5}$, is several magnitudes lower than typical values (10^{-2}–10^{-1}) found in giant H II regions in nearby galaxies (Kennicutt 1984). There is a suggestion that f is considerably lower for very compact H II regions. Kennicutt (1984) found for the H II region M82 A a value $f \geq 1.5 \times 10^{-4}$. Tenorio-Tagle (1994) has studied the dependence of the filling factor of star-forming clouds on the velocity dispersion of supersonic turbulence motions in the gas and has found that $f = M_{\rm Mach}^{-4}$, where $M_{\rm Mach}$ is the Mach number equal to the ratio of the shock velocity over the sound speed of the ambient gas. We do not know the velocity dispersion in Mrk 996, but, if we take the half-velocity width $\Delta v = 450$ km s^{-1} of the N III] λ1750 line as a characteristic value for the velocity of shocks and adopt a sound speed of 15.7 km s^{-1} at $T_e = 15{,}000$ K, we derive $f = 1.5 \times 10^{-5}$. Therefore, we conclude

TABLE 4
H II REGION MODEL PARAMETERS

PARAMETER	MODELS 1	MODELS 2
Q(H)(s^{-1})[a]	52.8	52.8
$T_{\rm eff}$ (K)[b]	47,000	47,000
log $r_{\rm in}$ (cm)[c]	18.4	18.4
log $r_{\rm out}$ (cm)[d]	21.0	21.0
α[e]	−2.0	−2.0
log N_0 (cm^{-3})[f]	6.66	6.66
log N_1 (cm^{-3})[g]	2.65	2.65
log f[h]	−4.58	−4.58
log (He/H)	−1.07	−1.07
log (C/H)	−4.54	−4.50
log (N/H)	−4.94	−4.11
log (O/H)	−4.04	−4.00
log (Ne/H)	−4.74	−4.70
log (Si/H)	−5.41	−5.41
log (S/H)	−5.60	−5.60
log (Fe/H)	−5.26	−5.26

[a] Log of number of ionizing photons per second.
[b] Effective temperature of ionizing stars.
[c] Inner radius of H II region.
[d] Outer radius of H II region.
[e] Defined by $N_e = N_0(r/r_{\rm in})^{-\alpha}$ in high-excitation zone.
[f] $N_0 = N_e(r_{\rm in})$.
[g] Constant density of low-excitation zone.
[h] Filling factor.

that a low-f value for the extremely compact nuclear H II region in Mrk 996 is not unreasonable.

Examination of Table 3 shows that both models generally reproduce well the line intensities in the optical range, except for the He I λ4471 and λ5876 lines, which will be discussed later. The derived oxygen abundance in both models is ∼1/10 of the solar value. The nitrogen abundance in model 1 has been set to ∼4 times the abundance derived in BCDs by Thuan et al. (1995) in order to reproduce the [N II] λ6584 line intensity. But even with this N abundance increase, the model predicts a [N II] λ5755 line intensity too low by a factor ∼5. In the UV wavelength range, the agreement between the observed and predicted Si III] λ1895 and C III] λ1909 line intensities is reasonable, but both models predict a O III] λ1663 line intensity ∼2 times higher than the observed one, and model 1 predicts a N III] λ1750 line intensity ∼6 times lower than that observed. Model 2 was constructed to remedy the latter problem. Its nitrogen abundance was increased to 6 times that of model 1, i.e., to ∼25 times the mean value derived for BCDs (Thuan et al. 1995). The predicted N III] λ1750 in model 2 is then in good agreement with the observed value. The high-N abundance implies that, in model 2, N^{++} ions are as important coolants as C^{++} and O^{++} ions.

The line intensities of all other high-excitation nebular lines and of the [O III] λ4363 and [N II] λ5755 are also well reproduced by model 2. However, the predicted line intensity of the nebular [N II] λ6584 line, which is produced in the outer low-excitation zone, is too large by a factor of ∼5.6 in model 2, while it is well reproduced by model 1 with a lower nitrogen abundance. Thus, to reproduce all nitrogen line intensities, both for the semiforbidden and auroral lines in the high-excitation region and for the nebular lines in the low-excitation region, the most natural way would be to invoke a hybrid model combining the features of both models 1 and 2, i.e., a high-nitrogen abundance in the high-density, high-excitation inner region and a low-nitrogen abundance in the low-density, low-excitation outer region. The [N II] λ5755/λ6584 intensity ratio yields $N_e \sim 10^5$ cm^{-3}. This density is not real because the two lines originate in different regions, but it does imply that most of the [N II] λ5755 emission comes from a region with $N_e \gg 10^5$ cm^{-3} and that most of the [N II] λ6584 emission comes from $N_e \ll 10^5$ cm^{-3}. This H II region model with a N abundance gradient is supported by the detection of WN stellar features in the spectrum of Mrk 996. WN stars would pollute the inner region with nitrogen from their stellar winds. The mass motions induced by these stellar winds would also account for the larger width of the N III] λ1750 line formed in the vicinity of the WR stars, as compared with the C III] λ1909 line formed farther out in a lower density region.

We caution the reader that there are many input parameters to models 1 and 2 and that these models may not be unique. Nevertheless, we feel that the general features of the hybrid model, a density gradient and nitrogen abundance gradient set up by stellar winds from WR stars located in the densest part of the star-forming region, will remain. We can bolster our confidence in our hybrid model by deriving the C/O and N/O abundance ratios by another method, using, exclusively, the semiforbidden UV lines O III] λ1663, N III] λ1750, and C III] λ1909. Although these lines arise in the inner high-density ($N_e \sim 10^6$ cm^{-3}) region, because they are semiforbidden, the usual methods for deriving abundances in the low-density limit ($N_e \leq 10^8$ cm^{-3}) can be applied. Furthermore, these lines are close to each other in wavelengths, so that their line ratios are extinction independent, unlike the models ran with CLOUDY, where we had to assume that the UV extinction was less than the extinction derived from the Balmer decrement. To calculate the C and N abundances relative to O, we follow the procedure in Garnett et al. (1995):

$$\frac{C^{++}}{O^{++}} = 0.089 \exp\left(-\frac{1.09}{t}\right)\frac{I(\lambda1909)}{I(\lambda1663)}, \quad (5)$$

$$\frac{N^{++}}{O^{++}} = 0.212 \exp\left(-\frac{0.043}{t}\right)\frac{I(\lambda1750)}{I(\lambda1663)}, \quad (6)$$

where $t = 10^{-4}\,T_e$. While equation (5) was derived for the low-density limit, it also applies at high densities. For $N_e \sim 10^6$ cm^{-3}, it underestimates the C/O ratio by a factor of only ∼1.07. The reason is that, although at those densities the C III] λ1906 gets collisionally de-excited, most of the de-excitations end up in the upper state of C III] λ1909, so that the C III] λ1906 + λ1909 is almost unaffected (Peimbert 1995). We take $t = 1.5$, as given by the model calculations with CLOUDY. This yields $C^{++}/O^{++} = 0.41$ and $N^{++}/O^{++} = 1.01$. Adopting ionization correction factors ICF(C) ∼ 1 (Garnett et al. 1995) and ICF(N) ∼ 1, we derive log (C/O) = −0.4 and log (N/O) = 0.0 for Mrk 996. These derived abundances are in good general agreement with those found in model 2 (Table 4), giving us confidence that our CLOUDY models, the adopted UV extinction, and the high-nitrogen abundance derived in model 2 for the inner high-density region, which we attribute to pollution by WN stars, are correct. The (C/O) ratio derived for Mrk 996 is slightly higher than the value log (C/O) = −0.6 derived from the relation by Garnett et al. (1995) at the oxygen abundance of the BCD [log (O/H) = −4].

We can estimate the number ratio of late nitrogen WR stars (WNL) to O stars using the relation given by Vacca & Conti (1992):

$$\frac{N_{\rm WNL}}{N_{\rm O7V}} \approx \left\{0.35\left[\frac{L({\rm H}\beta)}{L(\lambda 4686)}\right] - 1.68\right\}^{-1} . \quad (7)$$

We can only give an upper limit to this ratio because only a lower limit to the Hβ luminosity $L(\mathrm{H}\beta)$ can be obtained with our observations. This is because of two reasons. First, our spectroscopic observations were obtained through an aperture of 0".86 diameter, smaller than the ~6" diameter of the nuclear star-forming region, leading to an underestimation of the Hβ luminosity by a factor ≤2. Second, the H II region in Mrk 996 is probably not ionization-bounded but density-bounded as discussed before. In that case, the observed Hβ luminosity gives a flux of ionizing photons that is underestimated. Comparison of the latter with the ionizing flux from the CLOUDY models (Q in Table 4) shows that the underestimation factor is ~1.5. Plugging the observed $L(\mathrm{H}\beta)$ in equation (7) gives N(WNL)/N(O7V) = 0.38. When the 1.5 underestimation factor is taken into account, this ratio becomes 0.25. This is a very large ratio, even if we take into account the aperture effect on the Hβ luminosity, which would give a ratio ≥0.1. Evolutionary population synthesis models (Cerviño & Mas-Hesse 1994; Leitherer & Heckman 1995) for galaxies with $Z_{\odot}/10$ (the metallicity of Mrk 996) predict a ratio of ~0.02. There is thus a ≥5 discrepancy factor between the observed and predicted number of WR stars. Maeder & Meynet (1994) have suggested that binary mass transfer can increase the number of WR stars, but it is not clear whether this mechanism can account for such a large factor.

By measuring the intensities of the He II λ4686 line produced by WNL stars and of the C IV λ5808 line produced by WC stars, we can estimate N(WC)/N(WR), the ratio of the number of WC stars to the total number of WR stars. Assuming that the luminosity in the He II λ4686 line of a single WNL star is 1.7×10^{36} ergs s^{-1} and that of the C IV λ5808 line in a single WC4 star is 2.5×10^{36} ergs s^{-1} (Vacca & Conti 1992), we derive N(WNL) = 601, N(WC) = 74, and N(WC)/[N(WNL) + N(WC)] = 0.11. This value is ~2 times lower than that given by Cerviño & Mas-Hesse (1994) for the metallicity of Mrk 996.

Finally, we discuss the helium abundance in Mrk 996. We have already noted that CLOUDY models fail to reproduce the He I λ4471 and λ5876 line intensities, underestimating them by factors of ~1.8 and ~1.4, respectively. This suggests that CLOUDY does not correctly take into account the collisional and fluorescent enhancement processes for the He I recombination lines. We take into account these processes using the formulae for collisional enhancement by Kingdon & Ferland (1995) and calculations for fluorescent enhancement by Robbins (1968). To correct for both effects, we need to derive three quantities in the He^+ zone: the electron temperature $T_e(\mathrm{He}^+)$, the electron number density $N_e(\mathrm{He}^+)$, and the optical depth $\tau(\lambda 3889)$ in the H II region for the He I λ3889 radiative transition. To solve for these three unknowns, we have the three He I line intensity ratios $I(\lambda 3889)/I(\lambda 5876)$, $I(\lambda 4471)/I(\lambda 5876)$, and $I(\lambda 6678)/I(\lambda 5876)$. The two latter ratios can be immediately derived from Table 3. The intensity of the He I λ3889 line is more of a problem because it is blended with hydrogen H8 λ3889 emission line. Since at high densities I(H8 λ3889)/I(Hβ) = 0.110 (Brocklehurst 1971), Table 3 gives I(He I λ3889)/I(Hβ) = 0.018 and He I $I(3889)/I(\lambda 5876)$ = 0.09. In the high-density limit, the collisional enhancement of He I recombination lines is independent of N_e (Kingdon & Ferland 1995). Furthermore, the collisional enhancement for the He I λ3889 and λ5876 lines is nearly the same (Kingdon & Ferland 1995). Therefore, the He I $I(\lambda 3889)/I(\lambda 5876)$ ratio is mainly dependent on the optical depth $\tau(\lambda 3889)$. We wish to derive $T_e(\mathrm{He}^+)$ and $\tau(\lambda 3889)$ so as to get the best agreement between the individual values of the ionized helium abundance $y^+ \equiv \mathrm{He}^+/\mathrm{H}^+$ for each of the He I λ4471, λ5876, and λ6678 lines, after correction for enhancement effects. The results of the calculations for three different electron temperatures $T_e(\mathrm{He}^+)$ are shown in Table 5. It is evident that y^+ derived from the He I λ4471 line is higher than the ionized helium abundances derived from the other two He I lines. This higher value can be due to the contamination of the He I λ4471 line by the [Fe II] λ4475 emission line. This is not implausible since other [Fe II] lines from the same multiplet, λ4287 and λ4452, and probably λ4414, are seen in the spectrum of Mrk 996 (Fig. 9). We thus exclude the He I λ4471 line and search for the best agreement between $y^+(\lambda 5876)$ and $y^+(\lambda 6678)$. Given an electron temperature $T_e(\mathrm{He}^+)$, this agreement is achieved by varying $\tau(\lambda 3889)$. The discriminator between the three different solutions presented in Table 5 is the He I $I(\lambda 3889)/I(\lambda 5876)$ intensity ratio. In that table, we also show the predicted He I $I(\lambda 3889)/I(\lambda 5876)$ ratios as derived from Robbins (1968). The best agreement between the observed and predicted $I(\lambda 3889)/I(\lambda 5876)$ ratios is for $T_e(\mathrm{He}^+)$ = 14,000 K. This value is very close to the mean value of $T_e(\mathrm{He}^+)$ = 14,300 K obtained with CLOUDY calculations, giving us confidence that quantities derived with CLOUDY are correct.

Since the nuclear H II region in Mrk 996 is ionized by hot stars with $T_{\rm eff}$ = 47,000 K (Table 4), the He^+ and H^+ zones

TABLE 5

HELIUM MASS FRACTION Y

Parameter	Electron Temperature $T_e(\mathrm{He}^+)$ 13,000 K	14,000 K	15,000 K
$y^+(\lambda 4471)$	0.115 ± 0.041	0.111 ± 0.040	0.107 ± 0.038
$y^+(\lambda 5876)$	0.088 ± 0.007	0.089 ± 0.008	0.089 ± 0.008
$y^+(\lambda 6678)$	0.088 ± 0.014	0.089 ± 0.014	0.089 ± 0.014
$\tau(\lambda 3889)$	67	48	30
$I(\lambda 3889)/I(\lambda 5876)$[a]	0.06	0.10	0.22
Y[b]	0.262 ± 0.027	0.263 ± 0.028	0.264 ± 0.028

[a] Predicted value from Robbins 1968 calculations.
[b] Weighted mean from all three He I lines.

are nearly coincident (Stasinska 1990). In this case, the fraction of neutral helium is small and we can set ICF(He) to 1. The helium mass fraction can be calculated by

$$Y = \frac{4y[1 - 20(O/H)]}{1 + 4y}, \quad (8)$$

where $y = \mathrm{ICF(He)}y^+$ (Pagel et al. 1992). The mean value of Y in Table 5 is 0.263 ± 0.027. This helium mass fraction is somewhat larger than that derived in other BCDs with comparable metallicities by Izotov et al. (1994, 1995). The enhanced helium mass fraction in Mrk 996 is not surprising since some pollution from Wolf-Rayet stars is to be expected, as is the case with nitrogen.

4. SUMMARY

We have analyzed WFPC2 V and I images and FOS UV and optical spectrophotometry obtained with the refurbished *HST* of the unusual blue compact dwarf galaxy Mrk 996. We have derived the following results:

1. Mrk 996 is a dwarf galaxy ($M_B \sim -16.7$) with a nuclear starburst in the center of a stellar disk. The surface brightness profile for radii larger than 7″ can be well fitted by an exponential law with a very small scale length (0.42 kpc) and a B central surface brightness of 20.3 mag arcsec^{-2}, much brighter than the central surface brightness of normal spirals and low surface brightness dwarf spirals. There is a faint bulge component most evident in the region with radii between 3″ and 7″.

There is a tiny two-arm spiral-like structure. It is not seen over the whole disk but is confined to the inner 160 pc in radius. The $(V-I)$ color of the disk is that of a K1 main sequence or G5 giant star. Mrk 996 has a hydrogen mass of $1.1 \times 10^8\ M_\odot$, corresponding to a gaseous mass fraction of ~ 0.26.

2. The spiral-like structure is connected to the nuclear star-forming region that is extremely compact, with a radius of ~ 315 pc. The star-forming region is not at the center of the outermost elliptical isophote. There is a distinct asymmetry, the envelope being more extended to the northeast side than to the southwest side. There being no obvious sign of tidal interaction with a nearby companion, the asymmetry might be caused by a past merger. There are dust patches $\sim 2''$ north of the nuclear star-forming region.

3. Projected against and around the galaxy are many pointlike sources that can be interpreted as old ($\geq 10^{10}$ yr) globular clusters, as evidenced by their color [$(V-I)_0 \sim 0.9$], absolute magnitude range ($-10.4 \leq M_V \leq -6.8$), and unresolved diameters (≤ 20 pc). In the $-0.9 \leq M_V \leq -7.5$ range, the globular cluster luminosity function in Mrk 996 is remarkably similar to that of the Milky Way. There is a suggestion that Mrk 996 has slightly more clusters at the bright end of the globular cluster luminosity function than the Milky Way. There is a distinct assymmetry in the spatial distribution of globular clusters around Mrk 996, with the majority of them to the south of the galaxy, perhaps an effect of the same past merger responsible for the asymmetry of the outer parts.

4. The UV and optical spectra of the nuclear star-forming region of Mrk 996 show remarkable features, suggestive of very unusual physical conditions as compared with other emission-line dwarf galaxies. In the UV range, the N III] λ1750 and C III] λ1909 lines are particularly intense, while the O III] λ1663 line is weak. The N III] λ1750 has a broader width (FWHM ~ 900 km s^{-1}) than the other UV lines. In the optical range, the He I line intensities are particularly large. Emission lines of low-ionization ions (O^+, S^+, N^+) have narrower line widths than those of higher ionization stages (all helium lines, the Ne^{++} and O^{++} lines, and all auroral lines) that also have line widths of ~ 900 km s^{-1}. The optical spectra show WR features. We derive the number ratio of late-type WN stars to O stars to be ≥ 0.1, larger by a factor of ≥ 5 than predictions by evolutionary synthesis models. The ratio of the number of WC stars to the total number of WR stars is ~ 0.11.

5. We found that the usual low-density ionization-bounded H II region model cannot be applied to the nuclear star-forming region of Mrk 996 without leading to unrealistic helium and heavy-element abundances. Instead, a central compact density-bounded H II region model is more appropriate. In this model, the nuclear H II region has a very high density ($N_e \geq 10^6$ cm^{-3}), as suggested by the galaxy's morphology, and a density gradient caused by outflow motions due to WR stellar winds, as suggested by the large widths (~ 900 km s^{-1}) of the high-excitation lines. Using the CLOUDY program, we were able to find H II region models that adequately reproduced the observed line intensities, but with two added assumptions. First, the UV extinction is lower than the one derived using the Balmer decrement. This is reasonable since dust is efficiently destroyed or removed in the vicinity of O stars by ionizing radiation, stellar winds, and supernovae. Second, the nitrogen abundance decreases from the inner high-excitation zone to the outer low-excitation zone by a factor of ~ 6. This is reasonable given the pollution of the inner zone by stellar winds from WN stars. That pollution is also responsible for the very high nitrogen abundance in the center, ~ 25 times larger than that derived in other blue compact galaxies. The oxygen abundance of Mrk 996 is $\sim 1/10$ that of the Sun, log (C/O) $= -0.6$. Its helium mass fraction is $Y \sim 0.26$, slightly higher than in other BCDs at comparable metallicities, but not surprising, since some pollution from WR stars is to be expected.

T. X. T. acknowledges the partial financial support of NASA grant NAG 5-2060 and STScI grant GO 5408.01-93A. Y. I. I. is grateful for the hospitality of the Astronomy Department of the University of Virginia. This international collaboration was made possible by NATO collaborative research grant 921285. We thank Jean-Michel Martin and Simon Pustil'nik for sharing with us the H I observations of Mrk 996. We are grateful to Manuel Peimbert for useful comments on the manuscript.

REFERENCES

Bessell, M. S. 1990, PASP, 102, 1181
Brocklehurst, M. 1971, MNRAS, 153, 471
Burstein, D., & Heiles, C. 1982, AJ, 87, 1165
Cerviño, M., & Mas-Hesse, J. M. 1994, A&A, 284, 749
Danziger, I. J. 1983, in Supernova Remnants and Their X-Ray Emission, ed. J. Danziger & P. Gorenstein (Dordrecht: Reidel), 193
Denisyuk, E. K., & Lipovetsky, V. A. 1984, Astrophysics, 20, 290
Fanelli, M. N., O'Connell, R. W., & Thuan, T. X. 1988, ApJ, 321, 768
Feibelman, W. A., Aller, L. H., & Hyung, S. 1992, PASP, 104, 339
Ferland, G. J. 1993, Univ. of Kentucky, Dept. of Phys. and Astron. Internal Rep.
Freeman, K. C. 1970, ApJ, 160, 811

Garnett, D. R., Skillman, E. D., Dufour, R. J., Peimbert, M., Torres-Peimbert, S., Terlevich, R., Terlevich, E., & Shields, G. A. 1995, ApJ, 443, 64

Harris, W. E. 1991, ARA&A, 29, 543

Harris, H. C., Hunter, D. A., Baum, W. A., & Jones, J. H. 1993, AJ, 105, 1196

Holtzman, J. A., Burrows, C. J., Casertano, S., Hester, J. J., Trauger, J. T., Watson, A. M., & Worthey, G. 1995, PASP, 107, 1065

Hyung, S., Aller, L. H., & Feibelman, W. A. 1994, ApJS, 93, 465

Izotov, Yu. I., Lipovetsky, V. A., Guseva, N. G., & Kniazev, A. Yu. 1992, in The Feedback of Chemical Evolution on the Stellar Content of Galaxies, ed. D. Alloin & G. Stasinska (Paris: Paris Obs. Publ.), 138

Izotov, Yu, I., Guseva, N. G., Lipovetsky, V. A., Kniazev, A. Yu., Neizvestny, S. I., & Stepanian, J. A. 1993, Astron. Astrophys. Trans., 3, 197

Izotov, Yu. I., Thuan, T. X., & Lipovetsky, V. A. 1994, ApJ, 435, 647

———. 1995, in Interplay between Massive Star Formation, the ISM and Galaxy Evolution, ed. D. Kunth, B. Guiderdoni, M. Heydari-Malayeri, & T. X. Thuan (Gif-sur-Yvette: Editions Frontières)

Kennicutt, R. C. 1984, ApJ, 287, 116

Kingdon, J., & Ferland, G. J. 1995, ApJ, 442, 714

Landolt, A. U. 1992, AJ, 104, 340

Leitherer, C., & Heckman, T. M. 1995, ApJS, 96, 9

Lipovetsky, V. A., Thuan, T. X., Richter, G. M., Pustil'nik, S. A., & Izotov, Yu. I. 1995, in preparation

Loose, H.-H., & Thuan, T. X. 1985, in Star-Forming Dwarf Galaxies and Related Objects, ed. D. Kunth, T. X. Thuan, & J. T. T. Van (Gif-sur-Yvette: Editions Frontières), 73

Loose, H.-H., & Thuan, T. X. 1986, ApJ, 309, 59

Lutz, J. H., Kaler, J. B., Shaw, R. A., Schwarz, H. E., & Aspin, C. 1989, PASP, 101, 966

Maeder, A., & Meynet, G. 1994, A&A, 287, 803

Markarian, B. E., Lipovetsky, V. A., & Stepanian, J. A. 1977, Astrophysics, 13, 215

Pagel, B. E. J., Simonson, E. A., Terlevich, R. J., & Edmunds, M. G. 1992, MNRAS, 255, 325

Peimbert, M. 1995, private communication

Pustil'nik, S. A., Ugryumov, A. V., Lipovetsky, V. A., Thuan, T. X., & Guseva, N. G. 1995, ApJ, 443, 499

Robbins, R. R. 1968, ApJ, 151, 511

Rocca-Volmerange, B., Prévot, L., Ferlet, R., Lequeux, J., & Prévot-Burnichon, M. L. 1981, A&A, 99, L5

Schombert, J. M., Pildes, R. A., Eder, J. A., & Oemler, A., Jr. 1995, AJ, 110, 2067

Stasinska, G. 1990, A&AS, 83, 501

Seaton, M. J. 1979, MNRAS, 187, 73

Tenorio-Tagle, G. 1994, in Violent Star Formation from 30 Doradus to QSOs, ed. G. Tenorio-Tagle (Cambridge: Cambridge Univ. Press), 50

Thuan, T. X., & Martin, G. E. 1981, ApJ, 247, 823

Thuan, T. X., Izotov, Yu. I., & Lipovetsky, V. A. 1995, ApJ, 445, 108

Thuan, T. X., Lipovetsky, V. A., Martin, J.-M., & Pustil'nik, S. A. 1995, A&AS, submitted

Vacca, W. D., & Conti, P. S. 1992, ApJ, 401, 543

Whitford, A. E. 1958, AJ, 63, 201